ANALYSIS OF HIGH SPEED THERMAL CHARACTERISTICS OF V-SHAPED POCKET CYLINDRICAL ROLLER BEARING

Jie HUANG [1], Yanbin LIU [2,*], Xuying LI[1]

The cylindrical roller bearing with V-shaped pocket has good anti-skidding performance, but the characteristics of frictional heat generation between the roller and pocket are still unclear. Therefore, this paper established the analysis model of bearing dynamics and frictional power loss based on the tribological principle, multi-body dynamics theory, to study the influence of different geometric parameters of V-shaped pocket on pocket frictional heat generation, and the V-shaped pocket geometric parameters were optimized by the orthogonal test method, the frictional heat generation characteristics of the optimized bearing pocket and various components were discussed. The findings indicate that the frictional heat generation of the V-shaped pocket is significantly influenced by its geometric features, and the frictional heat generation rises with the increase of rotation speed and load; the pocket frictional heat generation and overall frictional heat generation of the optimized bearing under high speed and light load operating condition are lower than that of the ordinary bearing.

Keywords: Cylindrical roller bearing; V-shaped pocket; Geometric parameter; Orthogonal test method; Frictional heat generation.

Nomenclature			
n	pocket wall (n=a, b, c, d)	T_{Iri}	the *i-th* roller and the inner ring raceway tangential friction force
σ	pocket clearance	T_{Ori}	the *i-th* roller and the outer ring raceway tangential friction force
x_{ri}	moving component of the roller mass center in the direction of x_i in the ideal coordinate system	F_{ari}	normal contact force between the *i-th* roller and the pocket wall a
ψ_i	angular displacement of the roller mass center	F_{bri}	normal contact force between the *i-th* roller and the pocket wall b
Δ_{cl}	minimum oil film thickness	F_{cri}	normal contact force between the *i-th* roller and the pocket wall c
δ	offset value	F_{dri}	normal contact force between the *i-th* roller and the pocket wall d

[1] School of Mechatronics Engineering, Henan University of Science and Technology, Luoyang 471003, China
[2] Henan Collaborative Innovation Center of Machinery Equipment Advanced Manufacturing, Henan University of Science and Technology, Luoyang 471003, China
* Corresponding author: Yanbin Liu, liuyb2018@haust.edu.cn

η	lubricant viscosity	T_{ari}	tangential friction force between the *i-th* roller and the pocket wall a
v_i, $v_{\mathrm{p}i}$	tangential speed of the roller and pocket wall, respectively	T_{bri}	tangential friction force between the *i-th* roller and the pocket wall b
l	roller length	T_{cri}	tangential friction force between the *i-th* roller and the pocket wall c
K	line contact stiffness coefficient	T_{dri}	tangential friction force between the *i-th* roller and the pocket wall d
C	Lee-wang damping coefficient	κ_{c}	cage angular displacement
μ	friction coefficient	τ_i	initial rotation angle of the roller
C_o	radial clearance	F_b	contact force between the cage and ring guide surface
$\boldsymbol{r}_b$	coordinate array at the center of the cage	m_b	cage mass
B	width of the guiding surface	I_b	cage rotational inertia
ε	centroid eccentricity of the cage	$\ddot{\psi}_b$	angular displacement of the geometric center of the cage pocket
σ_b	cage guide clearance	g	acceleration of gravity
D_b	guiding surface diameter	D_r	roller diameter
ω_b	cage angular speed	r_{i}	inner ring raceway radius
Δ_{cg}	critical value of oil film thickness	r_{o}	outer ring raceway radius
h_{cg}	minimum clearance between cage and guide surface	r	roller radius
m_r	roller mass	n_i	inner ring rotation speed
I_r	roller rotational inertia	n_{mi}	roller rotation speed
ω_{mi}	roller rotation angular speed	n_{ri}	roller rotation speed
x_{ir},y_{ir}	inner ring center of mass in the inertial coordinate system *X*, *Y* coordinates	D_{m}	pitch circle diameter
x_i, y_i	the *i-th* roller center of mass in the ideal coordinate system *X, Y* coordinates	υ	lubricating oil and gas mixture density
x_k, y_k	the *i-th* roller center of mass in the centroid coordinate system *X*, *Y* coordinates	C_v	lubricant adhesion drag coefficient
F_{Iri}	the *i-th* roller and the inner ring raceway normal contact force	ω_{ri}	roller angular speed
F_{Ori}	the *i-th* roller and the outer ring raceway normal contact force	ω_i	inner ring angular speed

1. Introduction

The cylindrical roller bearings are used as the key component of support and motion transmission for aero-engine spindles, and their performance directly affects the reliability and service life of the whole machine[1]. At high speed and light load operating conditions, cylindrical roller bearings often appear skidding phenomenon. The intense collision and friction between bearing components in contact with each other lead to serious frictional heat generation of bearings, resulting in the rise of bearing temperature, structural thermal deformation, and bearing jamming. According to statistics, 25% of the failure of aero-engine main shaft bearings is caused by frictional heat generation between the bearing components[2]. Therefore, the research on frictional heat generation characteristics of cylindrical roller bearing under high-speed and light-load has important practical significance. Wang et al.[3] established the quasi-static analysis model of cylindrical roller bearing, considered the interaction of various contact forces and friction forces inside the bearing, and studied the frictional heat generation of heat sources such as inner and outer ring raceway, cage pocket, and guide surface of the outer ring. Chen et al.[4] have studied the effects of ball spin heat generation, ball and inner and outer ring raceway sliding frictional heat generation, and cage and ring guide surface frictional heat generation based on the proposed static mechanics and frictional heat analysis model of ball bearings, and the effects of different operating conditions on the local frictional heat generation and total frictional heat generation of each bearing component was investigated. Ma et al.[5] proposed a spherical roller bearing frictional heat generation model and analyzed the frictional power loss generated by the contact of roller and ring raceway, roller and cage pocket, and cage and inner ring guide surface, and roller oil churning power loss, studied the influence of rotation speed, load, radial clearance, etc. on frictional heat generation of the bearing. Wang et al.[6] proposed the pseudo-static analysis model to analyze frictional heat generation between cage and ring guide surface, ball and cage pocket, etc, under different rotational speeds and loads. They obtained that the change of speed and axial load greatly impacts the frictional heat generation of each bearing component, while the shift in radial load has a smaller impact. Li et al.[7] established the frictional power loss model of high rotation speed and light load rolling bearing considering bearing slippage. The result shows that the frictional heat generation of the inner and outer ring increase with the increase in slip rate. However, the frictional heat generation of the cage guide surface and roller stirring show the opposite trend. Takabi et al.[8] established an analysis model of bearing frictional power loss and studied the frictional heat generation caused by roller and inner ring raceway, cage and guide surface, and viscous resistance of lubricating oil. Ghaisas et al.[9] established a six-degree of freedom cylindrical roller model, studied the effects of pocket clearance and internal clearance on cage stability under

the operating condition of high speed and light load, and defined the quantitative measurement of cage stability. Selvaraj et al.[10] developed a cylindrical roller bearing test bench, derived dimensionless parameters that affect cage slip, and studied the effects of parameters such as radial load, shaft speed, viscosity, number of rollers, and bearing temperature on cage slip rate. Gupta[11] used simulation software ADORE to conduct simulation analysis on cylindrical roller bearing, and studied the influence of friction relationship at the contact points between the roller and the ring raceway, the roller and the cage on bearing performance. Patel et al.[12] established a nonlinear dynamics model of cylindrical roller bearing based on the contact force between the roller and the inner and outer ring raceway, and predicted the nonlinear stiffness and damping between the components of the cylindrical roller bearing by establishing the roller-raceway contact model.

In summary, the research on frictional heat generation of cylindrical roller bearings at home and abroad mainly focuses on roller and ring raceway, cage and ring guide surface. At the same time, there is a lack of frictional heat generation research on the cage pocket of cylindrical roller bearings, and analysis of the thermal characteristics of bearings with particular pocket structures is rare. The V-shaped pocket cylindrical roller bearing has good stability and anti-skidding performance[13]. However, the effect of the V-shaped pocket geometric parameters on frictional heat generation remains unclear.

This paper takes advantage of the V-shaped pocket structure of the cage to establish the bearing thermal analysis model based on multi-body dynamics theory and tribological principle. The impact of different pocket geometric parameters on the pocket frictional heat generation under high rotation speed and light load conditions was discussed, and the frictional heat generation characteristics of the bearing with optimized geometry parameters were studied. The research results of this paper provide a theoretical basis for the study of the thermal characteristics of cylindrical roller bearings with V-shaped pocket.

2. Thermal analysis model of V-shaped pocket bearing

2.1. Cylindrical roller bearing V-shaped pocket structure

The cylindrical roller bearing V-shaped pocket structure is shown in Fig. 1, Where O_r is the roller center of mass, α is the inclination angle of the pocket a and c walls, β is the inclination angle of the pocket b and d walls. The V-shaped pocket structure has better positioning and guiding accuracy for the roller in the radial plane, which can reduce the collision frequency between the roller and the pocket in the movement process.

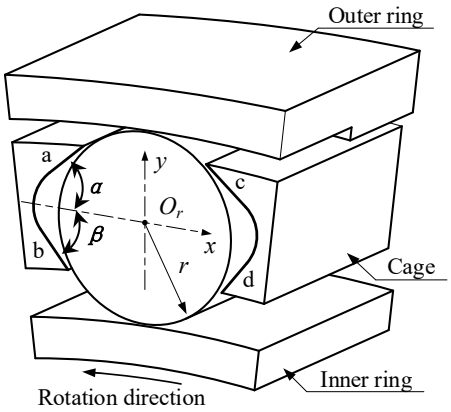

Fig 1. Schematic diagram of V-shaped pocket structure

2.2. Dynamic analysis model of bearing

(1) Roller and pocket contact model

The cylindrical roller bearing contact model between the roller and the V-shaped pocket is shown in Fig. 2. $\{O,x,y\}$ is the geometric center coordinate system of the pocket. $\{O,x_i,y_i\}$ is the ideal coordinate system of the roller, which is determined by the actual position of the roller in motion. $\{O_k,x_k,y_k\}$ is the roller centroid coordinate system. When the roller contacts the pocket wall, the contact deformation between the roller and the pocket wall is caused by the interaction of normal contact force and tangential friction force. When the roller is not in contact with the pocket wall, only hydrodynamic pressure exists between them[14]. Due to the bearing mainly enduring the radial load, to reduce the workload, it is assumed that the outer ring is fixed and the inner ring rotates, and plane constraints are imposed on the rollers and cage so that the whole bearing moves in the radial plane.

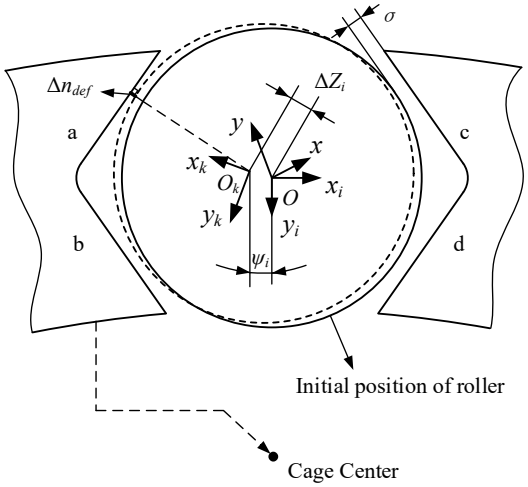

Fig 2. Contact model of roller and V-shaped pocket

The minimum clearance between the roller and the pocket wall is

$$\Delta n_{def}=\Delta Z_i-\sigma \tag{1}$$

Where ΔZ_i is the absolute value of the circumferential component of the roller center of mass in the ideal coordinate system, which can be expressed as

$$\Delta Z_a=\Delta Z_c=x_{\mathrm{r}i}\cdot\cos\psi_i\cdot\sin\alpha$$

$$\Delta Z_b=\Delta Z_d=x_{\mathrm{r}i}\cdot\cos\psi_i\cdot\sin\beta$$

When the minimum oil film thickness $\Delta_{\mathrm{cl}}\geq\Delta n_{\mathrm{def}}\geq 0$ between the roller and the pocket wall, the normal contact force between the roller and the pocket wall by the combined effect of Hertz line contact and hydrodynamic pressure is

$$F_{nri}=K_{\mathrm{cl}}\delta_{nri}^{10/9}+C_{\mathrm{cl}}\delta_{nri}^{10/9}\dot{\delta}_{nri}+\frac{2.44\eta\left|v_i+v_{\mathrm{p}i}\right|rl}{\Delta_{\mathrm{cl}}} \tag{2}$$

Where $\delta_{nri}=\Delta_{\mathrm{cl}}-\Delta n_{def}$; $K_{\mathrm{cl}},C_{\mathrm{cl}}$ is the line contact stiffness coefficient[15] and Lee-wang damping coefficient[16] between the roller and the pocket wall, respectively.

The friction force between the roller and the pocket wall is

$$T_{nri}=\mu_n F_{nri} \tag{3}$$

Where according to the sliding friction relationship between the roller and the pocket wall, μ_n is taken as 0.16.

When $\Delta n_{\mathrm{def}}>\Delta_{\mathrm{cl}}$, the normal contact force between the roller and the pocket wall under hydrodynamic pressure is

$$F_{nri}=\frac{2.44\eta\left|v_i+v_{\mathrm{p}i}\right|rl}{\Delta_{\mathrm{cl}}} \tag{4}$$

The friction force between the roller and the pocket wall is

$$T_{nri}=\frac{1.16\Delta_{\mathrm{cl}}F_{nri}\left|v_i-v_{\mathrm{p}i}\right|}{\left|v_i+v_{\mathrm{p}i}\right|\Delta n_{def}r^{1/2}} \tag{5}$$

(2) Roller and ring raceway contact model

The contact between the roller and the ring raceway is considered as a combination of Hertz line contact and lubrication friction, with a normal contact force is

$$F_{Nri}=K_{\mathrm{rl}}\delta_{Nri}^{10/9}+C_{\mathrm{rl}}\delta_{Nri}^{10/9}\dot{\delta}_{Nri} \tag{6}$$

Where *N*=*I*, *O*; For the roller and the inner ring raceway, $\delta_{Iri}=r+R_i-\left|\boldsymbol{r}_i-\boldsymbol{r}\right|$, $\boldsymbol{r}=[0\quad -e]^{\mathrm{T}}$, for the roller and the outer ring raceway, $\delta_{Ori}=\left|\boldsymbol{r}_i\right|-R_i-r-C_o$; $K_{\mathrm{rl}},C_{\mathrm{rl}}$ is the line contact stiffness coefficient and Lee-wang damping coefficient between the roller and the ring raceway, respectively.

The friction force between the roller and ring raceway is

$$T_{Nri}=\mu_N F_{Nri} \tag{7}$$

Where μ_N can be calculated based on the model proposed by Sekiya[17].

(3) Cage and ring guide surface contact model

When there is no contact between the cage and the ring guide surface, there is only hydrodynamic pressure between the cage and the ring guide surface. The contact force between the cage and the ring guide surface can be expressed as

$$F_b = -\begin{bmatrix} F_e & F_o \\ -F_o & F_e \end{bmatrix} \frac{\boldsymbol{r}_b}{e} \tag{8}$$

$$F_e = \frac{\eta D_b \omega_b B^3}{2\sigma_b^2} \frac{e^2}{\left(1-e^2\right)^2};\ F_o = \frac{\eta D_b \omega_b B^3}{8\sigma_b^2} \frac{\pi e}{\left(1-e^2\right)^{3/2}};\ e = \varepsilon - \sigma_b$$

When the cage and the ring guide surface come into contact, they can be equivalent to the combined action of Hertz contact and hydrodynamic pressure. At this time, the contact force between the cage and the ring guide surface can be expressed as

$$F_b = -\begin{bmatrix} F_e & F_o \\ -F_o & F_e \end{bmatrix} \frac{\boldsymbol{r}_b}{e} - \begin{bmatrix} F_n & F_t \\ -F_t & F_n \end{bmatrix} \frac{\boldsymbol{r}_b}{e} \tag{9}$$

$$F_n = K_{\mathrm{cg}} \delta_{\mathrm{cg}}^{10/9} + C_{\mathrm{cg}} \delta_{\mathrm{cg}}^{10/9} \dot{\delta}_{\mathrm{cg}};\ F_t = \mu_n F_n$$

Where $\delta_{\mathrm{cg}} = \Delta_{\mathrm{cg}} - h_{\mathrm{cg}}$; $K_{\mathrm{cg}}, C_{\mathrm{cg}}$ is the line contact stiffness coefficient and Lee-wang damping coefficient between the cage and the ring guide surface, respectively.

(4) Dynamic equation of roller

Newton's equation for the *i-th* roller is

$$\begin{aligned} m_r \ddot{\boldsymbol{r}}_i = m_r g [0 \quad -1]^{\mathrm{T}} &+ \frac{F_{Iri}(\boldsymbol{r}_i - \boldsymbol{r}_{ir})}{\left|\boldsymbol{r}_{ir} - \boldsymbol{r}_i\right|} + \frac{T_{Iri}(\boldsymbol{p}_i - \boldsymbol{p}_{ir})}{\left|\boldsymbol{p}_i - \boldsymbol{p}_{ir}\right|} \\ &+ \mathrm{sgn}(V_{Ori}) T_{Ori}\, \boldsymbol{p}_i / \left|\boldsymbol{p}_i\right| + F_{ari}\gamma_a + F_{bri}\gamma_b \\ &+ F_{cri}\gamma_c + T_{cri}\xi_c + F_{cri}\gamma_d + T_{dri}\xi_d - \frac{F_{Ori}\boldsymbol{r}_i}{\left|\boldsymbol{r}_i\right|} \\ &- T_{ari}\xi_a - T_{bri}\xi_b \end{aligned} \tag{10}$$

$$\gamma_a = [-\cos(\kappa_{\mathrm{c}} + \tau_i - \alpha) \quad -\sin(\kappa_{\mathrm{c}} + \tau_i - \alpha)]^{\mathrm{T}};\ \gamma_b = [\cos(\kappa_{\mathrm{c}} + \tau_i + \beta) \quad -\sin(\kappa_{\mathrm{c}} + \tau_i + \beta)]^{\mathrm{T}}$$

$$\gamma_c = [-\cos(\kappa_{\mathrm{c}} + \tau_i + \alpha) \quad \sin(\kappa_{\mathrm{c}} + \tau_i + \alpha)]^{\mathrm{T}};\ \gamma_d = [\cos(\kappa_{\mathrm{c}} + \tau_i - \beta) \quad \sin(\kappa_{\mathrm{c}} + \tau_i - \beta]^{\mathrm{T}}$$

$$\xi_a = [\sin(\kappa_{\mathrm{c}} + \tau_i - \alpha) \quad -\cos(\kappa_{\mathrm{c}} + \tau_i - \alpha)]^{\mathrm{T}};\ \xi_b = [\sin(\kappa_{\mathrm{c}} + \tau_i + \beta) \quad \cos(\kappa_{\mathrm{c}} + \tau_i + \beta)]^{\mathrm{T}}$$

$$\xi_c = [\sin(\kappa_{\mathrm{c}} + \tau_i + \alpha) \quad \cos(\kappa_{\mathrm{c}} + \tau_i + \alpha)]^{\mathrm{T}};\ \xi_d = [\sin(\kappa_{\mathrm{c}} + \tau_i - \beta) \quad -\cos(\kappa_{\mathrm{c}} + \tau_i - \beta)]^{\mathrm{T}}$$

$$\boldsymbol{r}_i = [x_i \quad y_i]^{\mathrm{T}}, \boldsymbol{r}_{ir} = [x_{ir} \quad y_{ir}]^{\mathrm{T}};\ \boldsymbol{p}_i = [-y_k \quad x_k]^{\mathrm{T}}, \boldsymbol{p}_{ir} = [e_{\mathrm{i}} \quad 0]^{\mathrm{T}}$$

Euler's equation for the *i-th* roller is

$$\begin{aligned} I_r \dot{\omega}_{mi} = r[&\mathrm{sgn}(V_{Iri}) T_{Iri} - \mathrm{sgn}(V_{Ori}) T_{Ori} \\ &- T_{ari} - T_{bri} - T_{cri} - T_{dri}] \end{aligned} \tag{11}$$

(5) Dynamic equation of cage

Newton's equation of the cage is

$$\begin{aligned} m_b\ddot{\boldsymbol{r}}_c &= F_{b\mathrm{g}} + m_b g[0 \quad -1]^{\mathrm{T}} \\ &- \sum_{i=1}^{n}\left(F_{ari}\gamma_a + F_{bri}\gamma_b - T_{ari}\xi_a - T_{bri}\xi_b\right) \\ &- \sum_{i=1}^{n}\left(F_{cri}\gamma_c + F_{dri}\gamma_d + T_{cri}\xi_c + T_{dri}\xi_d\right) \end{aligned} \tag{12}$$

Euler's equation of the cage is

$$\begin{aligned} I_b\ddot{\psi}_b = &\sum_{i=1}^{n}\{F_{ari}(\boldsymbol{r}_i - \boldsymbol{r}_c)^{\mathrm{T}}\xi_a + F_{bri}(\boldsymbol{r}_i - \boldsymbol{r}_c)^{\mathrm{T}}\xi_b \\ &- F_{cri}(\boldsymbol{r}_i - \boldsymbol{r}_c)^{\mathrm{T}}\xi_c - F_{dri}(\boldsymbol{r}_i - \boldsymbol{r}_c)^{\mathrm{T}}\xi_d\} - m_b g \\ &- \sum_{i=1}^{n}\{(T_{ari} + T_{cri})[(r_{\mathrm{i}} + r + \tfrac{1}{2}\delta_0)\sin\alpha - (r+\sigma)] \\ &- (T_{bri} + T_{dri})[(r_{\mathrm{i}} + r + \tfrac{1}{2}\delta_0)\sin\beta + (r+\sigma)]\} \end{aligned} \tag{13}$$

Where $\boldsymbol{r}_c = [x_c \quad y_c]^{\mathrm{T}}$ is the X and Y coordinate components of the cage center in the inertia system.

2.3 Analysis model of bearing frictional power loss

The cylindrical roller bearing frictional power loss analysis model is shown in Fig. 3. The frictional power loss generated by each heat source due to the frictional heat generation includes[18]: roller and ring raceway, roller and pocket wall, cage and the ring guide surface between the sliding frictional power loss and roller oil churning frictional power loss. As the cylindrical roller bearing for the spindle of the aero-engine is mainly sustained to radial load during operation, the axial contact load between the roller end face and the ring raceway guide edge is slight. Therefore, the sliding frictional power loss of the roller end face and the ring raceway guide edge is ignored. The frictional power loss generated by each heat source can be calculated as

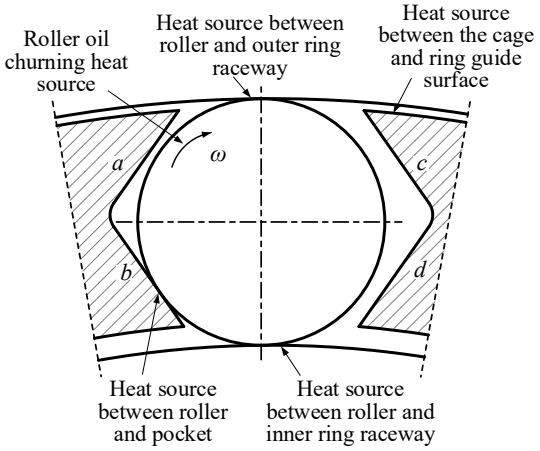

Fig 3. Analysis model of bearing frictional power loss

1) Sliding frictional power loss between the roller and pocket wall

Due to the change of contact position, the normal contact force and friction force between the roller and each pocket wall are different. Therefore, the sliding frictional power loss between the roller and the pocket can be represented as

$$H_{ni} = \sum_{i=1}^{n} \left(H_{ai} + H_{bi} + H_{ci} + H_{di} \right) \tag{14}$$

$$H_{a\lambda} = \frac{1}{2} D_r \omega_{mi} T_{ari} \quad H_{b\lambda} = \frac{1}{2} D_r \omega_{mi} T_{bri}$$

$$H_{ci} = \frac{1}{2} D_r \omega_{mi} T_{cri} \quad H_{di} = \frac{1}{2} D_r \omega_{mi} T_{dri}$$

2) Sliding frictional power loss of roller and ring raceway

$$H_{Ni} = \sum_{i=1}^{n} T_{Nri} V_{Nri} \tag{15}$$

Where V_{Nri} is the relative sliding speed of the *i-th* roller and the inner and outer ring raceway due to the rotation speed difference(N=I, O); According to the dynamic relationship between the components, the relative sliding speed between the roller and the inner and outer ring raceway can be expressed as

$$V_{Iri} = \frac{\pi}{30} (n_i - n_{mi}) r_{\mathrm{i}} - n_{ri} r$$

$$V_{Ori} = \frac{\pi}{30} (n_{mi} r_{\mathrm{o}} - n_{ri} r)$$

3) Frictional power loss of roller oil churning

$$H_{fi} = \sum_{i=1}^{n} \frac{1}{2} D_{\mathrm{m}} \frac{\upsilon C_v D_r (D_{\mathrm{m}} \omega_{ri})^{1.95}}{16g} \omega_{mi}^{0.81} \tag{16}$$

4) Sliding frictional power loss between cage and ring guide surface

$$H_g = \frac{1}{2} D_b F_b (\omega_b - \omega_i) \mu \tag{17}$$

5) Total frictional power loss of bearing

$$H_{total} = H_{ni} + H_{Ni} + H_{fi} + H_g \tag{18}$$

3 Frictional heat generation characteristics of V-shaped pocket

3.1 Verification of theoretical analysis model

Based on the main geometric parameters of the cylindrical roller bearing in reference[19], established the bearing's dynamics model and frictional power loss analysis model by using the above modeling methods. The frictional power loss of the bearing under different operating conditions is solved, and compared and analyzed the simulation data with the experimental data of bearing frictional heat generation in reference[19] to verify the reliability of the bearing thermal analysis

model proposed in this paper. Fig. 4 shows the comparison curve of the simulation and the experimental data of bearing frictional heat generation under different operating conditions. As can be seen from the figure, the simulation data of the bearing frictional heat generation obtained by using this paper's thermal analysis model are in good agreement with the reference's experimental data, indicating that the theoretical analysis model proposed in this paper has high reliability.

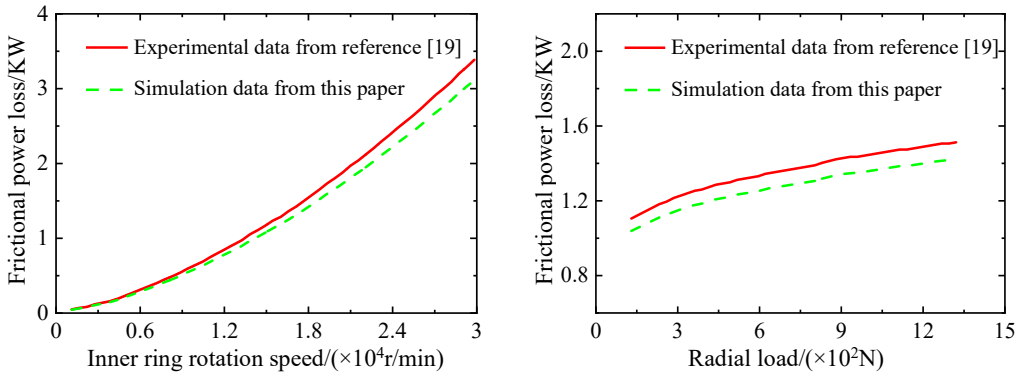

(a) Radial load 666N (b) Inner ring rotation speed 16800r/min

Fig 4. The bearing frictional heat generation under different operating conditions

3.2. Bearing main parameters and data processing

The cylindrical roller bearing main geometrical and material parameters are given in Table 1 and Table 2. The bearing is lubricated with 4109 aviation lubricating oil[20], and its parameters as seen in Table 3.

Table 1

Geometric parameters of the bearing

parameter	Numerical value
Inner ring diameter/mm	100
Outer ring diameter/mm	140
Bearing width/mm	20
Number of rollers	26
Roller diameter/mm	10
Roller length/mm	7
Cage inner diameter/mm	114.46
Cage outer diameter/mm	124.46

Table 2

Material parameters of the bearing

Component	Density /(kg/mm^3)	Elastic modulus /(N/mm^2)	Poisson's ratio
Inner ring	7.85E-06	2.07E+05	0.29
Outer ring	7.85E-06	2.07E+05	0.29
Roller	7.85E-06	2.07E+05	0.29
Cage	8.55E-06	1.06E+05	0.32

Table 3

Parameters of 4109 aviation lubricating oil

parameter	Numerical value
Density/(kg/mm^3)	8.6E-07
Viscosity/(Pa·s)	3.3E-02
Heat conduction coefficient/(N·s^{-1}·°C^{-1})	9.66E-02
Viscosity-pressure coefficient/(Pa^{-1})	1.28E-08
Viscosity-temperature coefficient/(°C^{-1})	3.2E-02

Fig. 5 shows the transient frictional heat generation curve between roller and pocket based on the analysis model of bearing dynamics and frictional power loss under the conditions of V-shaped pocket wall inclination angle α=40° and β=40°, inner ring speed 24000r/min and radial load 100N and 900N, respectively.

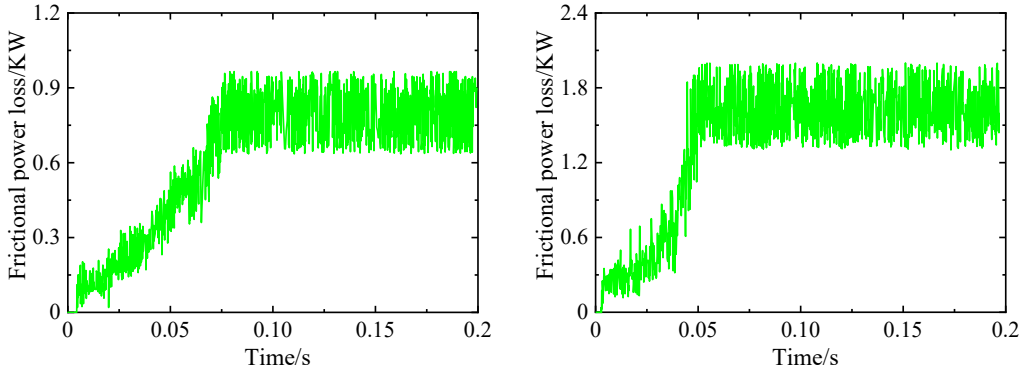

(a) Radial load 100N (b) Radial load 900N

Fig 5. Time variation curve of cage pocket frictional heat generation under different radial loads

According to the variation trend of pocket heat generation over time in Fig. 5, it can be seen that the change of time makes the frictional heat generation curve fluctuate continuously, which is not conducive to determining the specific frictional power loss of the pocket under a given operating condition. However, with the increase of time, the kinematic relationship between bearing components gradually tends to be stable, and the fluctuation amplitude of pocket frictional heat generation also gradually stabilized. Therefore, to highlight the influence of the pocket wall inclination angle on the frictional heat generation of the pocket and each bearing component under different rotation speeds and loads, and to stand out the key points, the mean value of the stable stage of the bearing transient frictional heat generation was used in this paper for the analysis of the results.

3.3 Effect of pocket geometry parameters on pocket frictional heat generation

(1) Effect of pocket geometry parameters on pocket frictional heat generation under different rotation speeds.

When the radial load is 100N, the rotation speed range of the inner ring is 12000 r/min~24000 r/min, the V-shaped pocket wall inclination angle α and β are taken to different values, and the roller and pocket frictional heat generation results are shown in Fig. 6.

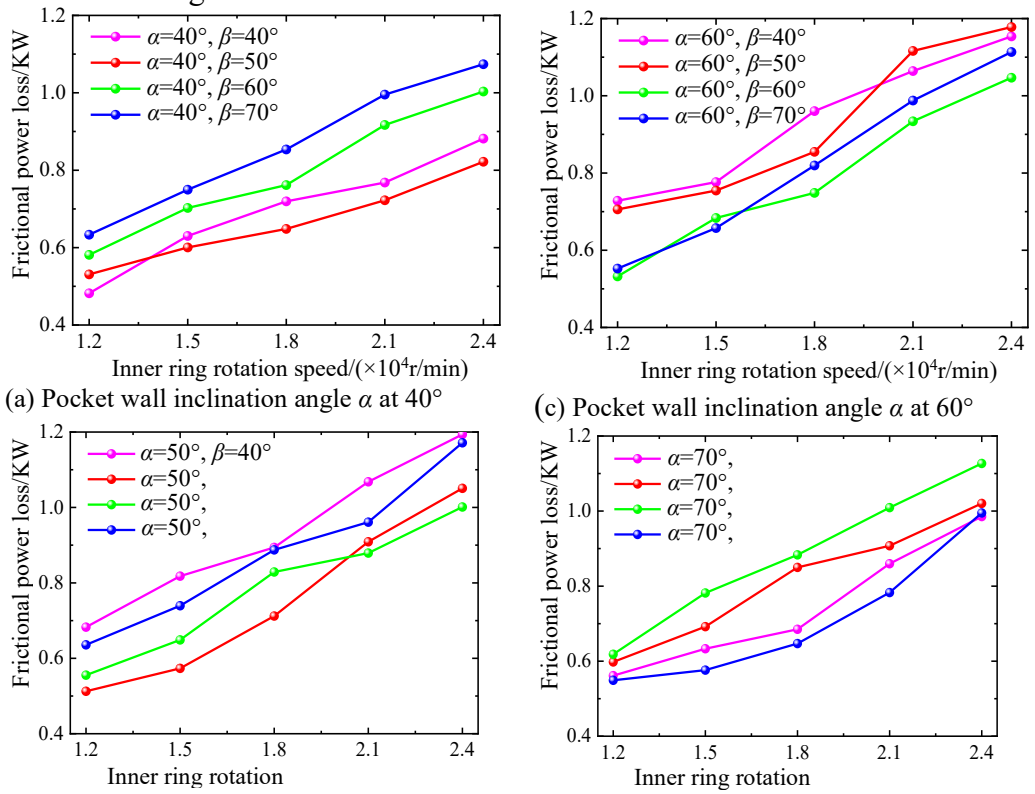

(a) Pocket wall inclination angle α at 40°

(c) Pocket wall inclination angle α at 60°

(b) Pocket wall inclination angle α at 50°

(d) Pocket wall inclination angle α at 70°

Fig 6. Effect of pocket geometry parameters on pocket frictional heat generation at different rotation speeds

According to Fig. 6, the frictional heat generation of the V-shaped pocket under different geometric parameters increases nonlinearly with the increase of rotation speed, because with the enhancement of rotation speed, the cage stability decreases, the sliding speed and friction force between the roller and the pocket increase, leading in the continuous increase of pocket frictional heat generation[21]. Under the operating conditions of the same radial load and different inner ring speeds, Fig. 6(a), (b), (c), and (d) respectively show the pocket frictional power loss when the pocket wall inclination angle α is given, and the pocket wall inclination angle β takes different values. When the inclination angle α remains constant, the

change of inclination angle β has a more significant influence on the pocket frictional heat generation, because the stability of the cage decreases with the increase of the inner ring rotation speed, and the larger the inclination angle β, the lower the positioning accuracy of the pocket, and the faster the collision frequency between the roller and the pocket. The constantly changing positional relationship makes severe sliding friction between the roller and the pocket, significantly increasing the pocket frictional heat generation.

(2) Effect of pocket geometry parameters on pocket frictional heat generation under different radial loads.

When the inner ring rotation speed is 24000r/min, the radial load range is 100N~900N, the V-shaped pocket wall inclination angle α and β are taken as different values, and the results of frictional heat generation between roller and pocket are shown in Fig. 7.

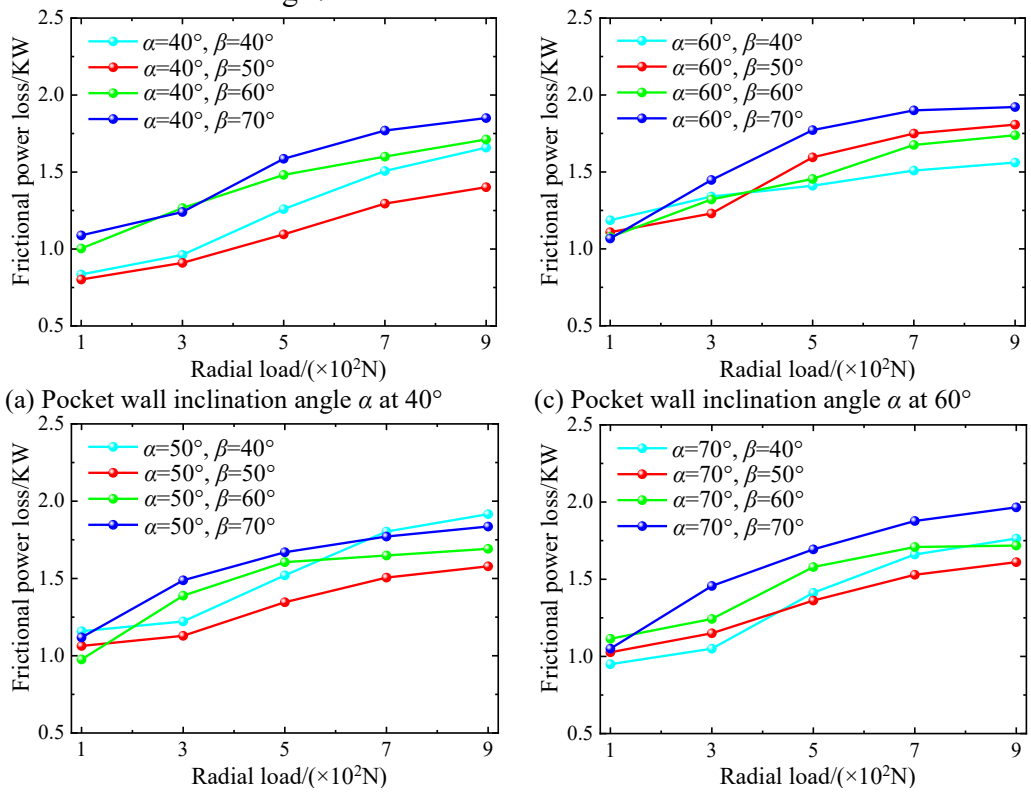

(a) Pocket wall inclination angle α at 40°

(c) Pocket wall inclination angle α at 60°

(b) Pocket wall inclination angle α at 50°

d) Pocket wall inclination angle α at 70°

Fig 7. Effect of pocket geometry parameters on pocket frictional heat generation under different radial loads

As seen in Fig. 7, with the increase in load, the frictional power loss of the pocket wall gradually increases and then flattens. This is because when the radial load is low, the slippage between the roller and the pocket is serious, and the sliding friction is high; When the radial load is further increased, the stability of the cage

increases, the slippage phenomenon is reduced, and the frictional heat generation is relatively reduced. Under the operating conditions of the same inner ring rotation speed and different radial loads, Fig. 7(a), (b), (c), and (d) respectively show the pocket frictional power loss when the pocket wall inclination angle α is given, and the pocket wall inclination angle β takes different values. A comprehensive view of the pocket wall frictional heat generation trend is similar, while when the wall inclination angle α remains constant, the increase of β gives rise to the increase of the relative position clearance between the roller and the pocket wall, at the same time, with the increase of the radial load, the collision frequency and interaction force of the roller and the pocket increases during the high rotation speed, exacerbating the collision sliding friction between the roller and the pocket, and causing the pocket frictional heat generation to increase. When the wall inclination angle β remains unchanged, the addition of the angle α leads to the increase of the pocket frictional power loss, because the addition of the wall inclination angle α essentially causes the movement of the roller in the circumferential plane, and the centrifugal force[22] generated in the high-speed rotation process causes the elastic hysteresis of the roller, increasing the contact force between the roller and the pocket, which has a significant impact on the frictional heat generation of the pocket.

3.4 V-shaped pocket geometric parameters optimization

The orthogonal test method is mainly used to study multi-level and multi-factor optimization problems due to its uniform distribution and neat comparability, which can effectively replace the optimization design of bearing pocket structure parameters[23]. Therefore, taking the V-shaped pocket frictional power loss as the target parameter and the pocket wall inclination angle as the influencing factor, the geometric parameters of the V-shaped pocket are optimized by the orthogonal test method to determine the optimal inclination angle of the V-shaped pocket wall. Because the radial load and rotation speed of the bearing will affect the frictional power loss of the pocket, only the influence of the different pocket wall inclination angles under the high speed, light load, and critical load on the pocket frictional power loss is considered during the optimization of the geometric parameters of the pocket.

According to the manufacturability of bearing in actual production, the optimization design range for each wall inclination angle of the V-shaped pocket is determined as follows:

$$\begin{cases} \alpha \in [40°,70°] \\ \beta \in [40°,70°] \end{cases}$$

Four levels are uniformly selected within the optimization design range of the pocket wall inclination angle for orthogonal test analysis. The factors and levels are shown in Table 4.

Table 4

Table of factors and levels of orthogonal test

Factor	Level			
	1	2	3	4
α	40	50	60	70
β	40	50	60	70

The orthogonal test table $L_{16}(4^2)$ is shown in Table 5 and Table 6. Table 5 shows the orthogonal test combination and results of pocket wall inclination angle under the light load of 100N and rotation speed of 24000r/min. Table 6 shows the orthogonal test combination and results of the pocket wall inclination angle at a critical load of 900N and rotation speed of 24000r/min.

Table 5

Orthogonal test combination I and results

Serial number	Wall inclination angle α/°	Wall inclination angle β/°	Frictional power loss /W
1	40	40	881.74
2	40	50	821.74
3	40	60	1003.28
4	40	70	1073.89
5	50	40	1193.65
6	50	50	1050.81
7	50	60	1001.21
8	50	70	1171.45
9	60	40	1153.67
10	60	50	1178.06
11	60	60	1046.67
12	60	70	1113.32
13	70	40	985.28
14	70	50	1020.39
15	70	60	1126.89
16	70	70	994.92

Table 6

Orthogonal test combination II and results

Serial number	Wall inclination angle α/°	Wall inclination angle β/°	Frictional power loss /W
1	40	40	1658.57
2	40	50	1401.64
3	40	60	1711.74
4	40	70	1850.83
5	50	40	1916.03
6	50	50	1578.40
7	50	60	1691.80
8	50	70	1836.26
9	60	40	1560.91

10	60	50	1807.28
11	60	60	1738.58
12	60	70	1922.16
13	70	40	1763.61
14	70	50	1610.59
15	70	60	1718.27
16	70	70	1965.65

As shown in Fig. 8, it can be seen that the change in the wall inclination angle of the V-shaped pocket leads to an obvious difference in the frictional power loss under the same operating condition by converting the results of each orthogonal test combination into a three-dimensional surface figure for intuitive comparative analysis. When the range of pocket wall inclination angle is $40°\leq \alpha <45°$, $45°\leq \beta <55°$, the frictional power loss of the pocket is relatively small. Therefore, α=40°, β=50° are used as the optimized V-shaped pocket wall inclination angle after comprehensive consideration of the results of pocket frictional heat generation and bearing manufacturability.

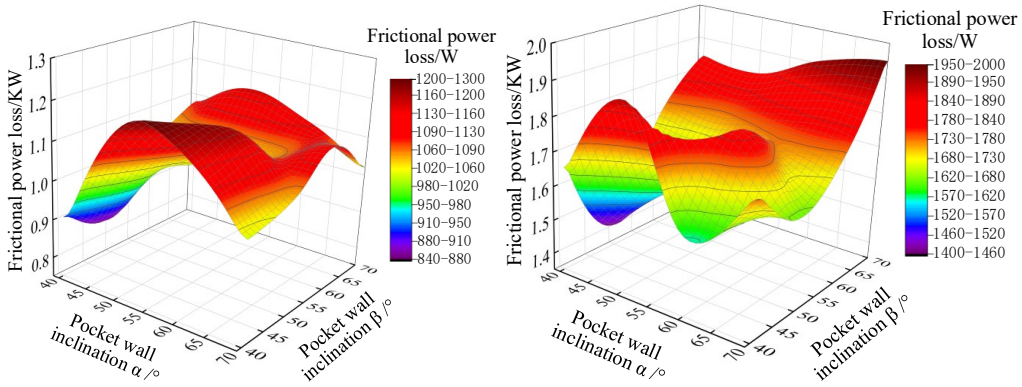

(a) Combination I (b) Combination II

Fig 8. Results of orthogonal test

4. Frictional heat generation characteristics on optimized bearing

To investigate the frictional heat generation characteristics of bearing with optimized geometry parameters of V-shaped pocket, compared and analyzed the frictional heat generation of optimized bearing and ordinary bearing with arc pocket under high rotation speed and light load, and the results are shown in Fig. 9 and Fig. 10.

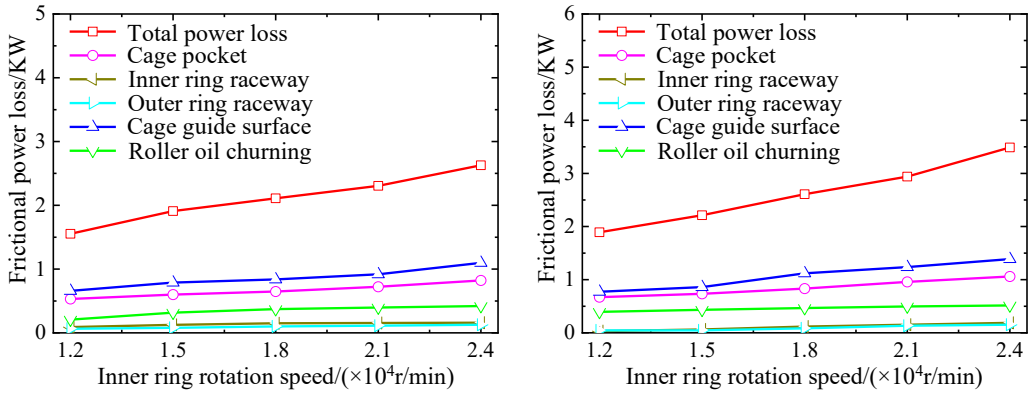

(a) Optimized bearing (b) Ordinary bearing

Fig 9. Comparison of frictional heat generation of bearings at different rotation speeds

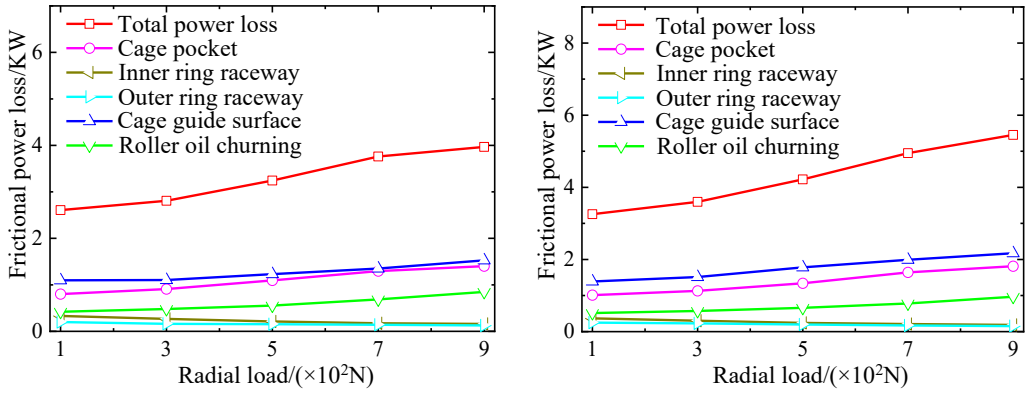

(a) Optimized bearing (b) Ordinary bearing

Fig 10. Comparison of frictional heat generation of bearings under different radial loads

The comparison of frictional heat generation between optimized and ordinary bearing under the radial load of 100N and rotation speed range of 12000r/min~24000r/min is shown in Fig. 9. It can be concluded that with the increase of the inner ring rotation speed, the frictional power loss of the roller and ring raceway increases less, the frictional power loss of the oil churning, the cage guide surface, and the roller and the pocket wall increases more. The pocket frictional power loss and total frictional power loss of the optimized bearing are lower than the ordinary bearing, as shown in Fig. 11(a) and (b), the reason is that with the increase of inner ring rotation speed, the collision frequency between the roller and pocket wall increases, resulting in the reduction of bearing stability. However, the contact state between the roller and the pocket is improved due to the better radial positioning of the roller by the V-shaped pocket structure, making the contact force between the optimized bearing roller and each wall of the pocket significantly lower than the ordinary bearing, which improves the stability of the optimized bearing at the high rotation speed, and inhibits the sliding friction

between the bearing components during the rotation process, thus reduces the frictional heat generation between the bearing components.

Fig. 10 is the bearing frictional heat generation contrast during the operating conditions of rotation speed 24000r/min, radial load range from 100N to 900N. As seen in the figure, at the high rotation speed, the increase in radial load increases the stability of the bearing, reducing sliding friction between various components, as a consequence, the frictional power loss of the bearing first rises and then flattens out. As shown in Fig.11(b) and (c), the increase in radial load also aggravates the contact force between the roller and the pocket wall. However, the stability of the ordinary bearing is lower compared to the optimized bearing, and the collision frequency between each wall of the pocket and the roller is significantly higher than that of the optimized bearing. Therefore, the optimized bearing can achieve a stable state faster than ordinary bearing in terms of the roller and cage rotation speed during operating conditions, reducing heat generation due to sliding friction between the roller and pocket under an unbalanced state. Meanwhile, the high stability of the optimized bearing also makes the frictional heat generation between various components lower than that of the ordinary bearing.

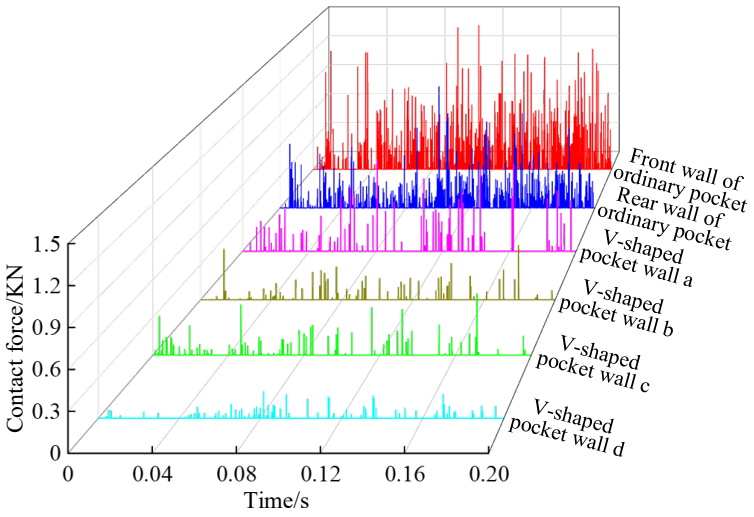

(a) Rotation speed 12000r/min and radial load 100N

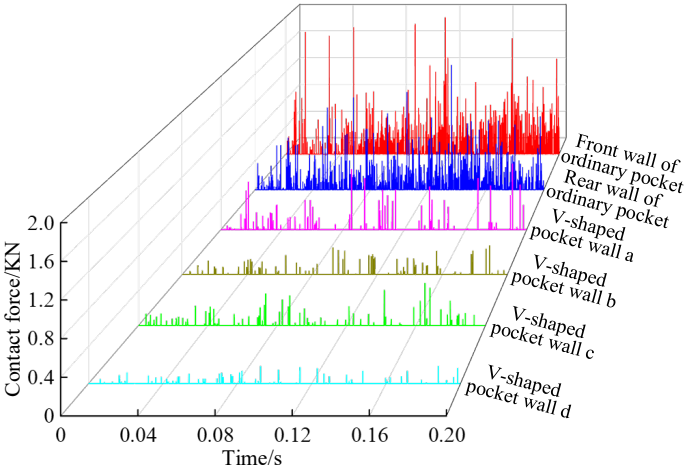

(b) Rotation speed 24000r/min radial load 100N

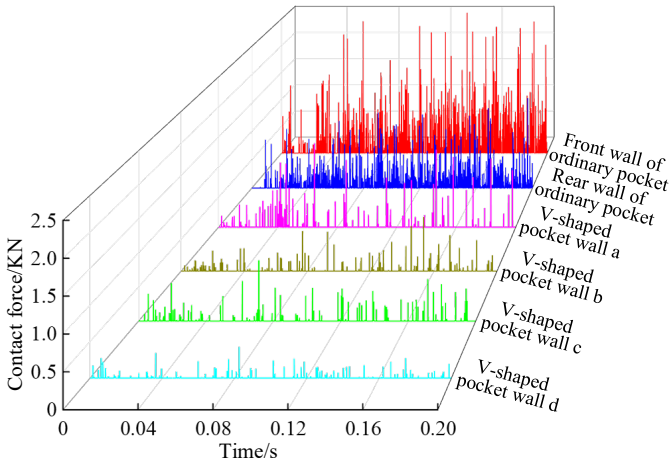

(c) Rotation speed 24000r/min radial load 900N

Fig 11. Comparison of contact force on the pocket wall of optimized bearing and ordinary bearing under different operating conditions

The change in the shape of the pocket inevitably leads to a change in the cage stability, so the cage slip rate[24] is used to evaluate the skidding degree of optimized and ordinary bearing. Fig. 12 shows the changing trend of the cage slip rate between the optimized and ordinary bearing when the radial load is 100N and the inner ring rotation speed range is 12000 r/min~24000 r/min. As can be seen from the figure, the cage slip rate of the optimized bearing is lower, and its stability is better than the ordinary bearing. The main problem caused by bearing slippage during operation is the thermal damage caused by the rigid contact area between the roller and ring raceway after the oil film rupture, which will lead to a sharp rise in temperature and rapidly transfer to the contact area of the bearing components[25]. However, the optimized bearing has a low slippage, which avoids

the bearing structural deformation due to the temperature rise of the components caused by bearing skidding, which will aggravate the frictional heat generation at the contact area of each component.

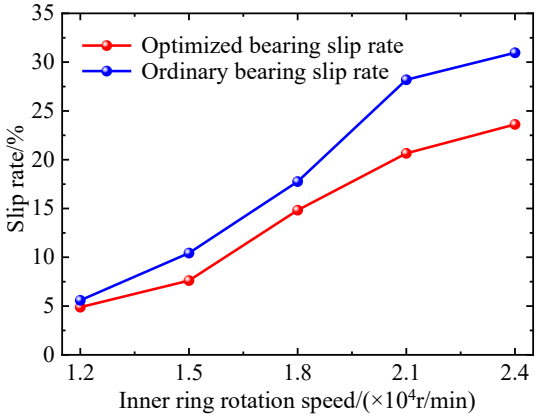

Fig 12. Comparison of cage slip rate at different rotation speeds

5. Conclusions

In this paper, the cylindrical roller bearing with V-shaped pocket is taken as the research object, the influence of different pocket geometric parameters on the frictional heat generation of the roller and the V-shaped pocket was considered by combined with the bearing dynamics and frictional power loss analysis model, which indicated that the inclination angle of the pocket wall of the V-shaped pocket significantly affects the frictional heat generation between the roller and the pocket; The V-shaped pocket wall inclination angle was optimized by the orthogonal test method under giving operating conditions, and the optimized V-shaped pocket geometric parameter α=40° and β=50° were obtained; And the difference between the optimized bearing and the ordinary bearing in terms of frictional heat generation and total frictional heat generation of each component was analyzed and compared, the result show that the frictional heat generation the optimized bearing are lower than those of the ordinary bearing.

Acknowledgment

The research was funded by the National Natural Science Foundation of China (Grant No.52175086).

REFERENCES

[1]. *H.F. Ding, F.T. Wang, M.Q. Jing, Y.S. Li and Y. Wang*, "The thermal stability of high-speed ball bearings", Journal of Vibration and Shock, **vol.36**, no.14, 2017, pp.168-173.

[2]. *K. Yan, Y.T. Wang, Y.S. Zhu, J. Hong and Q. Zhai*, "Investigation on heat dissipation characteristic of ball bearing cage and inside cavity at ultra-high rotation speed", Tribology International, **vol.93**, 2016, pp.470-481.

[3]. *L.Q. WANG, G.C. CHEN, L. GU and D.Z. Zheng*, "Study on heat generation of high-speed cylindrical roller bearings", Lubrication Engineering, **vol.192,** 2007, pp.8-11.
[4]. *G.C. CHEN, L.Q. WANG, L. GU and D.Z. Zheng*, "Heating analysis of the high speed ball bearing", Journal of Aerospace Power, **vol.22**, no.1, 2007, pp.163-168.
[5]. *F.B. Ma, Z.M. Li, B.J. Wu and Q. An*, "An accurate calculation method for heat generation rate in grease-lubricated spherical roller bearings", Proceedings of the Institution of Mechanical Engineers, Part J: Journal of Engineering Tribology, **vol.230**, no.4, 2016, pp.472-480.
[6]. *Y.S. Wang, H.F. Zhu and J. Liu*, "Finite element analysis on temperature field of bearing with shaft", Journal of Aerospace Power, **vol.27**, no.5, 2012, pp.1146-1152.
[7]. *J.N. Li, J.F. Xue and Z.T. Ma*, "Study on the thermal distribution characteristics of high-speed and light-load rolling bearing considering skidding", Applied Sciences, **vol.8**, no.9, 2018, pp.1593.
[8]. *J. Takabi and M.M. Khonsari*, "Experimental testing and thermal analysis of ball bearings", Tribology international, **vol.60**, 2013, pp.93-103.
[9]. *N. Ghaisas, C.R. Wassgren and F Sadeghi*, "Cage instabilities in cylindrical roller bearings", Journal of Tribology, **vol.126**, no. 4, 2004, pp.681-689.
[10]. *A. Selvaraj and R. Marappan*, "Experimental analysis of factors influencing the cage slip in cylindrical roller bearing", The International Journal of Advanced Manufacturing Technology, **vol.53**, 2011, pp.635-644.
[11]. *P.K. Gupta*, "On the frictional instabilities in a cylindrical roller bearing", Tribology transactions, **vol.33**, no.3, 1990, pp.395-401.
[12]. *U.K.A. Patel and S.H. Upadhyay*, "Nonlinear dynamic response of cylindrical roller bearing–rotor system with 9 degree of freedom model having a combined localized defect at inner–outer races of bearing", Tribology Transactions, **vol.60**, no.2, 2017, pp.284-299.
[13]. *Y.B. Liu, Z.H. Deng and D.Y. Sang*, "High-speed dynamic performance of cylindrical roller bearing with V-shape pocket", Acta Aeronautica et Astronautica Sinica, **vol.42**, no.7, 2021, pp.579-590.
[14]. *H. Wu and Q. An*, "Calculation on stiffness of cylindrical roller bearing with EHL", Bearing. **vol.338**, 2008, pp.1-4.
[15]. *J. Liu, Y.M. Shao, X M. Qin and J.J. Zhou*, "Dynamic modeling on localized defect of cylindrical roller bearing based on non-hertz line contact characteristics", Journal of. Mechanical Engineering, **vol.50**, no.1, 2014, pp.91-97.
[16]. *T.W. Lee and A.C. Wang*, "On the dynamics of intermittent motion mechanisms, Part 1: dynamic model and response", ASME Journal of Mechanisms, Transmissions and Automation in Design, **vol.105**, 1983, pp.534-540.
[17]. *M. Sekiya*, "Integrated bearing dynamic analysis system (IBDAS)", Technical Review, **vol.79**, 2011, pp.119-124.
[18]. *G.C. Chen*, Thermal analysis of high-speed rolling bearing used in main shaft of aeroengine, M.D. Thesis, Harbin Institute of Technology, 2008.
[19]. *R. Kerrouche, A. Dadouche, M. Mamou and S. Boukraa*, "Power Loss Estimation and Thermal Analysis of an Aero-Engine Cylindrical Roller Bearing", Tribology Transactions, **vol.64**, no.6, 2021, pp.1079-1094.
[20]. *Y.S. Wang, B.Y. Yang and L.Q. Wang*, "The study of rheological properties of aviation oil No.4109", Lubrication Engineering, **vol.30**, no.1, 2005, pp.55-58.
[21]. *S.E. Deng, Y.S. Hu, Y.F. Sun, J. Xu, R.J. Niu and Y.C. Cui*, "Analysis of frictional power loss characteristics of cylindrical roller bearing for air-conditioning vane compressor", Acta Armamentarii, **vol.40**, no.9, 2019, pp.1943-1952.
[22]. *L. Jin, Z.Y. Rui, H.Y. Jiang and J.L. Pan*, "Research on prediction of temperature rise of high speed angular contact ball bearing considering interaction between contact parameters and friction heat", Journal of. Mechanical Engineering, **vol.7**, 2021, pp.61-67.

[23]. *J.M. Zhang, M. Qiu and X.X.* Pang, "Structure optimization of cylindrical roller bearing based on orthogonal test", Journal of Mechanical Transmission, **vol.46**, no.3, 2022, pp.31-38.
[24]. *S.E. Deng, J.F. Gu, Y.C. Cui and C.Y. Sun*, "Analysis on dynamic characteristics of cage in high-speed cylindrical roller bearing", Journal of Aerospace Power, **vol.29**, no.1, 2014, pp.207-215.
[25]. *J.N. Li, W. Chen and Y.B. Xie*, "Experimental study on skid damage of cylindrical roller bearing considering thermal effect", Proceedings of the Institution of Mechanical Engineers, Part J: Journal of Engineering Tribology, **vol.228**, no.10, 2014, pp.1036-1046.